Available online at www.sciencedirect.com
ScienceDirect
Journal of Sound and Vibration 302 (2007) 67–87
JOURNAL OF SOUND AND VIBRATION
www.elsevier.com/locate/jsvi

Simplified calculation of structure-borne sound from an active machine component on a supporting substructure

A.T. Moorhouse*

Acoustics Research Centre, University of Salford, Manchester M5 4WT, UK

Received 6 July 2005; received in revised form 11 September 2006; accepted 7 November 2006
Available online 16 January 2007

Abstract

The background to the work is the increasing interest in virtual acoustic prototypes, and the need to predict sound pressure radiated from machines without having to assemble them physically. The focus of the paper is on structure-borne sound, and the objective is to investigate ways of simplifying the calculation of contact forces between a vibro-acoustically active component and its passive supporting structure. An analysis shows the importance of the singular values of the mobility matrices in determining the error due to simplifications. Errors are also analysed using Monte Carlo simulations for the case of an electric motor installed on a machine frame. The results show that at frequencies above the first anti-resonance, the off-diagonal elements of the source mobility matrix can be neglected. However, at lower frequencies no such simplification is possible. A hybrid mobility matrix is therefore proposed: at high frequencies it is diagonal, consisting of measured point mobilities, and at low frequencies the entire matrix is calculated using a simple rigid mass-stiffness model. Only point mobilities need to be measured rather than a full set of point and transfer mobilities, giving a significant reduction in measurement and data handling. Validation measurements show that the contact forces calculated using the hybrid matrix are, if anything, more accurate than those based on a purely measured matrix. It is argued that this is because the mass model is more robust than measured mobilities for this type of behaviour, being based on radii of inertia and mass only. It is noted that the conclusions are likely to apply to other structure-borne sound sources because of general similarities in low-frequency behaviour.

1. Introduction

The background to this paper is an increasing need for designers of machines to replace traditional physical prototypes by more cost-effective alternatives, most notably using 'virtual' technologies. In the field of acoustic design, there has been considerable interest in developing virtual acoustic prototypes as a faster and more cost-effective means of trying out new designs. Here, a machine that does not physically exist may be 'assembled' by combing, in the computer, sets of data that represent the appropriate vibro-acoustic properties of the separate components. The result may then be auralised to give a more or less realistic impression of the sound of the machine without the need to physically assemble it.

*Tel.: +44 161 295 5490.
E-mail address: A.T.Moorhouse@salford.ac.uk.

0022-460X/$ - see front matter
doi:10.1016/j.jsv.2006.11.022

In general, the external sound radiated from a machine may be due to initial excitation by fluctuating air pressure, vibration or time-varying pressure in fluids, i.e. by air-borne, structure-borne or fluid-borne excitation. In this paper only structure-borne excitation is considered, although the general scheme is applicable to all three excitation types. The machine is separated into two substructures: an active component that initially generates the disturbance, and the remaining passive parts of the machine frame which modify the sound by transmission and radiation. The overall aim is to predict the external radiated sound based on data obtained from the two separate subsystems before assembly. Since only structure-borne excitation is considered, we are looking specifically to predict the part of the external sound that is due to an initial structure-borne excitation by the active component.

The active component studied is an electric motor, which is rigidly bolted into the machine frame. Although a specific case, to a large extent this can be considered representative of a whole class of problems as will be discussed later.

The structure-borne sound source is considered as a 'black box', i.e. its effect on connected structures is represented by its properties at the connection points [1]. The properties required in this case are the mobility matrix of the connection points together with either the free velocity or the blocked force vector [2]. The mobility matrix of the receiving structure is also required in order to calculate the contact forces. The black box model assumes the excitation mechanisms inside the source remain invariant whatever the properties of the connected structure. This is probably not completely true in practical cases, but it is the most practical assumption in the absence of a detailed model of internal mechanisms, which does not exist for the majority of active components. There is an increasing number of studies where essentially this approach has been used to calculate the power transmitted to a passive receiver structure by a rigidly attached source, some examples of which are given in Refs. [2–6].

Although the black box model is now widely accepted, there is a practical problem in implementation because the amount of data required is large, particularly the mobility matrices [7,8]. Hence, the objective of this paper is to reduce the amount of data needed whilst maintaining an acceptable level of accuracy in the prediction of radiated sound.

2. Theory

2.1. Substructuring approach

In general, the sound pressure at various points around a machine can be represented as a column vector $\mathbf{p}$ of length m, where m is the number of receiver points. This is considered to be the result of n forces forming a length n vector, $\mathbf{f}$, acting on the machine frame (see Fig. 1). The force input and pressure output are linked by an $m \times n$ matrix of transfer functions $\mathbf{T}$ such that:

$$\mathbf{p} = \mathbf{T}\mathbf{f}. \tag{1}$$

Each element in $\mathbf{T}$ represents the sound pressure at external position j ($j = 1, 2, \ldots m$), per unit force excitation at point k ($k = 1, 2, \ldots n$) on the machine frame. $\mathbf{T}$ therefore represents the combined effect of all transmission

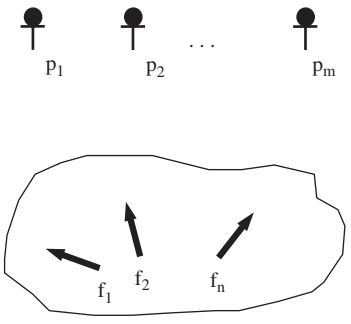

Fig. 1. Schematic of overall prediction scheme.

paths, and quantifies the net effect of vibration transmission through the frame, radiation from the frame and subsequent diffraction and transmission of the radiated sound on its way to the receiver position. Harmonic excitation is assumed, so all variables are functions of frequency.

The force vector $\mathbf{f}$ applied to the frame depends on both the source and receiver structure in general and is given by

$$\mathbf{f} = [\mathbf{Y}_S + \mathbf{Y}_R]^{-1}\mathbf{v}_{sf} \tag{2a}$$

in which $\mathbf{Y}_S, \mathbf{Y}_R$ are the mobility matrices of the source and receiver (frame) respectively, and $\mathbf{v}_{sf}$ is the vector of free velocities of the source. Eq. (2a) can also be written in terms of the blocked force vector by making the substitution $\mathbf{v}_{sf} = \mathbf{Y}_S\mathbf{f}_{sb}$ giving:

$$\mathbf{f} = [\mathbf{Y}_S + \mathbf{Y}_R]^{-1}\mathbf{Y}_S\mathbf{f}_{sb}, \tag{2b}$$

where $\mathbf{f}_{sb}$ is the vector of blocked forces which, like the free velocity, is an independent property of the source.

The difficulty in calculating external sound pressure stems largely from the difficulty in calculating the vector of contact forces. The overall aim of simplifying calculation of the sound pressure, $\mathbf{p}$, therefore largely equates with the problem of simplifying calculation of the forces. There are two main problems: firstly, the number of terms involved necessitates a significant measurement or calculation effort, which is not realistic for most industrial applications; secondly, a matrix inversion is involved which is associated with well-known numerical problems. Various ways of reformulating this problem have been investigated, such as use of eigenvalue decompositions [9–11] and other orthogonal transformations [12,13].

2.2. Estimation of error bounds

The question is now considered of how to determine the accuracy of simplified predictions. It is necessary to predict the sound pressure spectrum at typical listener positions around the machine from which the sound can be auralised [14,15]. Also of interest in most cases is the overall sound power of the assembled machine. The sound power provides the best overall indication that the acoustic behaviour has been accurately represented since it includes the effect of all points. Therefore, the sound power will be used as a reference quantity to assess the effect of simplifications. If the external receiver positions are chosen on the surface of a hemisphere or parallelpiped, then the sound power is proportional to the spatially averaged sound pressure squared. Therefore, the spatially averaged squared pressure is a suitable parameter to quantify the effect of simplifications. It can be written as the inner product of the pressure vector:

$$\sum_{j=1}^{m} |p_i|^2 = \mathbf{p}^H\mathbf{p} = |\mathbf{p}|^2 = \mathbf{f}^H\mathbf{T}^H\mathbf{T}\mathbf{f}, \tag{3a}$$

where $[\cdot]^H = [\cdot]^{*T}$ is the conjugate transpose, or Hermitian transpose. The right-hand side of Eq. (3a) can be expanded:

$$\sum_{j=1}^{m} |p_i|^2 = \sum_{j=1}^{m}\sum_{k=1}^{n}\sum_{i=1}^{n} T_{jk}^* T_{ji} f_k^* f_i = \sum_{j=1}^{m}\sum_{k=1}^{n} |T_{jk}|^2 |f_k|^2 + \sum_{j=1}^{m}\sum_{k=1}^{n}\sum_{\substack{i=1 \\ i\neq k}}^{n} T_{jk}^* T_{ji} f_k^* f_i, \tag{3b}$$

where f_i and T_{jk} are the elements of the force vector and transfer function matrix, respectively. For random excitation, the terms $|p_i|^2 = S_{p_i p_i}$ are the auto-spectra of the sound pressure at the external points, $|f_k|^2 = S_{f_k f_k}$ are the auto-spectra of the forces, and $f_k^* f_i = S_{f_k f_i}$ are the cross-spectra of the forces. Thus, Eqs. (3a) and (3b) express the energetically averaged external sound pressure in terms of the auto- and cross-spectra of the applied forces.

In the second form of Eq. (3b), the direct terms (first term) and cross terms (second term) have been separated out. If the forces are mutually incoherent, then the cross-spectra are zero and the cross terms vanish. In the following, it will be assumed that the forces are coherent, since this represents a worst case for the simplifications to be tested. However, it is worth noting at this stage that there are other conditions under which the cross terms may be negligible, even for coherent excitation. Firstly, if the phase of the product within the sum is random, then the sum of many terms will tend to zero. This will occur for example if the

receiver points are widely spaced compared with a wavelength. Secondly, if the phase varies with frequency (as would normally be expected) then a frequency average of the cross terms will tend to zero. Thirdly, if the magnitude of the off-diagonal transfer functions is small compared with that of the diagonal terms, as sometimes occurs then the resulting sum will be small.

Eqs. (3a) is recognised as a quadratic form. A standard procedure is to write the force vector as $\mathbf{f} = \mathbf{X}\mathbf{q}$ (in which the columns of $\mathbf{X}$ are the normalised eigenvectors of the $m \times m$ square matrix $\mathbf{T}^H\mathbf{T}$), so that the quadratic form is expressed as a weighted sum of eigenvalues [16]:

$$|\mathbf{p}|^2 = \sum_{i=1}^{n} |q_i|^2 \lambda_i, \tag{4a}$$

where the λ_i are the (non-negative) eigenvalues of the $m \times m$ square matrix $\mathbf{T}^H\mathbf{T}$ (which happen also to equal the squared singular values of $\mathbf{T}$ [16]). To illustrate the relationship between the magnitude of pressure and force, we write $q_i = a_i|\mathbf{q}|$ and note that $|\mathbf{q}|^2 = |\mathbf{f}|^2$ so as to obtain:

$$|\mathbf{p}|^2 = |\mathbf{f}|^2 \left(\sum_{i=1}^{n} |a_i|^2 \lambda_i \right), \tag{4b}$$

where $\sum_{i=1}^{n} a_i^2 = 1$, and $|\mathbf{f}|^2 = \sum_{i=1}^{n} |f_i|^2$. Eq. (4b) shows that the spatially averaged sound pressure squared (and hence sound power) is proportional to the spatially averaged force squared. Therefore, the following discussion is largely restricted to the problem of estimating the spatially averaged force magnitude squared $|\mathbf{f}|^2$.

The preceding development has been given in terms of forces, but the general approach is not restricted to forces and can also include moment excitation. This can be done by transforming the mobility matrix into a dimensionless form using the formulation described in Ref. [17], which is also given in Ref. [18]. The same steps as above can then be employed on the dimensionless matrix. For simplicity, the 'forces only' formulation will be continued in this paper.

With the above in mind, the effect of simplifications on the accuracy of the solution can be gauged by comparing the true modulus of the force vector $|\mathbf{f}|^2$ with that obtained from a simplified prediction denoted as $|\mathbf{f}'|^2$. Substituting for the forces from Eq. (2a), the ratio of approximate to true force squared is thus expressed as

$$E_v = \frac{|\mathbf{f}'|^2}{|\mathbf{f}|^2} = \frac{\mathbf{v}_{Sf}^H \left[\mathbf{Y}'_S + \mathbf{Y}'_R\right]^{-H} \left[\mathbf{Y}'_S + \mathbf{Y}'_R\right]^{-1} \mathbf{v}_{Sf}}{\mathbf{v}_{Sf}^H [\mathbf{Y}_S + \mathbf{Y}_R]^{-H} [\mathbf{Y}_S + \mathbf{Y}_R]^{-1} \mathbf{v}_{Sf}}, \tag{5a}$$

where $\mathbf{Y}'_S, \mathbf{Y}'_R$ are the simplified source and receiver mobility matrices, respectively, and the denominator represents the unmodified case. Alternatively, if the source is characterised by the blocked force then the normalised force squared follows from Eq. (2b) in a similar manner:

$$E_f = \frac{|\mathbf{f}'|^2}{|\mathbf{f}|^2} = \frac{\mathbf{f}_{Sb}^H \mathbf{Y}'^{\mathrm{H}}_S \left[\mathbf{Y}'_S + \mathbf{Y}'_R\right]^{-H} \left[\mathbf{Y}'_S + \mathbf{Y}'_R\right]^{-1} \mathbf{Y}'_S \mathbf{f}_{Sb}}{\mathbf{f}_{Sb}^H \mathbf{Y}_S^H [\mathbf{Y}_S + \mathbf{Y}_R]^{-H} [\mathbf{Y}_S + \mathbf{Y}_R]^{-1} \mathbf{Y}_S \mathbf{f}_{Sb}}. \tag{5b}$$

For a given source and receiver structure, the mobilities $\mathbf{Y}_S, \mathbf{Y}_R$, $\mathbf{Y}'_S, \mathbf{Y}'_R$ are of fixed value. However, the excitation vector ($\mathbf{f}_{Sb}$ or $\mathbf{v}_{sf}$) may vary for different speeds and running conditions of the source [19] and so in turn may the normalised force squared. Therefore, we need to consider the amplitude of the normalised force as a statistical quantity. Over certain frequency ranges, it is possible to place restrictions on the form of the excitation vector by bringing into play some knowledge of the source structure; for example, if the source is a rigid mass then the motion of each mount point is not independent (a detailed discussion of other such possibilities is given in Ref. [20]). However, rather than restrict the generality of the results it is assumed in the following that the excitation vector may take any form. Therefore, the ratio of approximate to true force must be given as a probability density at each frequency. This basic approach was first outlined in Ref. [21].

2.3. Errors in terms of mobility matrix singular values

In order to gain insight into the range of errors, it is noted that Eq. (5a) is the ratio of two positive semi-definite quadratic forms, each of which can be written as a weighted sum of eigenvalues:

$$E_f = \frac{|\mathbf{f}_{Sb}|^2 \sum_{i=1}^{m} \lambda'_{RS,i} |b'_i|^2}{|\mathbf{f}_{Sb}|^2 \sum_{i=1}^{m} \lambda_{RS,i} |b_i|^2}, \tag{6}$$

where $\lambda_{RS,i}$ are the eigenvalues of the $n \times n$ square matrix $[\mathbf{Y}_S + \mathbf{Y}_R]^{-H}[\mathbf{Y}_S + \mathbf{Y}_R]^{-1}$ (with units of 1/mobility squared) for the unmodified case, and similarly for $\lambda'_{RS,i}$; b'_i, b_i are the participation factors for the modified and unmodified mobility matrices, respectively, and $\sum_{i=1}^{n} b'^2_i = \sum_{i=1}^{n} b_i^2 = 1$ similarly to Eq. (4). In this case the eigenvectors correspond to spatial patterns in the free velocity at the contact points, and are functions of frequency.

It happens that since $[\mathbf{Y}_S + \mathbf{Y}_R]^{-H}[\mathbf{Y}_S + \mathbf{Y}_R]^{-1}$ is a Hermitian matrix, we have $\lambda_{RS,i} = 1/\sigma_i^2$, where the σ_i are the singular values of $[\mathbf{Y}_S + \mathbf{Y}_R]$, and similarly for the modified matrix. Substituting into Eq. (6) we obtain:

$$E_f = \sum_{i=1}^{m} \frac{|b'_i|^2}{\sigma'^2_i} \Bigg/ \sum_{i=1}^{m} \frac{|b_i|^2}{\sigma_i^2}. \tag{7}$$

The singular values can be thought of as an extension of the point mobility to multiple point contact: whereas the point mobility is the magnitude ratio of velocity to force at a point, the singular value is the ratio of spatially averaged velocity to spatially averaged force over multiple points when the spatial distribution of the exciting forces conforms to a particular spatial pattern (the corresponding singular vector) [10].

Eq. (7) is of the form of a singular value perturbation problem. It shows that the most important factor affecting the error is the change in the singular values when the matrix is 'perturbed', i.e. simplified, for example by removing elements (although the change in the singular vectors also plays a role). Problems of this type have been studied extensively, particularly in relation to numerical evaluation of singular values where the matrix is subject to a small error (see for example Ref. [22]).

It is possible to find bounds for the normalised force squared, since both the numerator and denominator are bounded by the maximum and minimum singular values:

$$\frac{1}{\sigma_{\max}^2} \leqslant \sum_{i=1}^{m} \frac{|b_i|^2}{\sigma_i^2} \leqslant \frac{1}{\sigma_{\min}^2}$$

and similarly for the modified case.

Therefore, strict upper and lower bounds for the normalised force squared can be given in terms of the ratio of singular values [10]:

$$\left(\frac{\sigma'_{\min}}{\sigma_{\max}}\right)^2 \leqslant E_f \leqslant \left(\frac{\sigma'_{\max}}{\sigma_{\min}}\right)^2. \tag{8}$$

This form is attractive for its simplicity and gives useful insight into the importance of the singular values in determining the bounds on the approximate solution. Furthermore, it can be written in terms of the singular values of the individual mobility matrices which is advantageous because they are independent properties of the source and receiver structure, respectively [10]. However, these forms are found to be of limited practical value in this case since the bounds are too conservative. Although there are perturbation methods that give less conservative bounds, these are most useful for small perturbations, typically considered to be of the order of numerical 'noise'.

2.4. Numerical evaluation of errors

For the much larger variations involved here, the approach with the least conservatism is the use of Monte Carlo methods. Similar methods were used in Ref. [23], where the variation in transmitted power was studied. The random variable in that case was taken to be the 'force ratios', i.e. the spatial variation of the contact forces, which are a property of both source and receiver. In the following, the variance in net contact force and

subsequent radiated sound pressure is to be studied in terms of the spatial patterns of free velocity. This has the advantage that free velocity is independent of the source and frame mobilities.

The free velocity vector can be written as

$$\mathbf{v}_{Sf} = |\mathbf{v}_{Sf}|\mathbf{q},$$

where $|\mathbf{v}_{Sf}| = (\sum_i |v_{Sf,i}|^2)^{1/2}$ is the length of the vector, $\mathbf{q} = \mathbf{q}_r + i\mathbf{q}_i$ and $\mathbf{q}^H\mathbf{q} = 1$, i.e. $\mathbf{q}$ is a normalised complex vector. Substituting into Eq. (5a) we obtain:

$$E_v = \frac{\mathbf{q}^H[\mathbf{Y}'_S + \mathbf{Y}'_R]^{-H}[\mathbf{Y}'_S + \mathbf{Y}'_R]^{-1}\mathbf{q}}{\mathbf{q}^H[\mathbf{Y}_S + \mathbf{Y}_R]^{-H}[\mathbf{Y}_S + \mathbf{Y}_R]^{-1}\mathbf{q}}, \tag{9a}$$

which shows that the normalised force squared is independent of the magnitude of the blocked force and depends only on the spatial patterns defined in $\mathbf{q}$. The corresponding error for the blocked force formulation is, from Eq. (5b):

$$E_f = \frac{\mathbf{q}^H\mathbf{Y}'^H_S[\mathbf{Y}'_S + \mathbf{Y}'_R]^{-H}[\mathbf{Y}'_S + \mathbf{Y}'_R]^{-1}\mathbf{Y}'_S\mathbf{q}}{\mathbf{q}^H\mathbf{Y}^H_S[\mathbf{Y}_S + \mathbf{Y}_R]^{-H}[\mathbf{Y}_S + \mathbf{Y}_R]^{-1}\mathbf{Y}_S\mathbf{q}}. \tag{9b}$$

Confidence limits for the approximate solution at each frequency can be obtained by solving Eqs. (9a) or (9b) many times for different $\mathbf{q}$, where the real and imaginary parts of $\mathbf{q}$ are random vectors.

3. Evaluation of errors using measured mobility matrices

This section contains a brief description of the measured mobilities, evaluation of the confidence limits for the approximate solution using both singular value and Monte Carlo methods, and interpretation of the results.

3.1. Mobility measurements

The source was an electric motor, suspended for measurement of mobility as illustrated in Fig. 2. Measurements were made at the four mounting locations and in the x, y and z directions. It was assumed that the coupling between the x, y and z directions was negligible, and rotational mobilities were not considered. The mobility matrix was therefore a 12×12 matrix with 3 blocks of 4×4 on the diagonal. The corresponding measurements were also made on the frame, a plastic washing machine tub.

In Fig. 3 (top) are shown some sample measured mobilities for the frame. The behaviour is mass-like up to 400 Hz where an anti-resonance occurs. Above 500 Hz some resonances of the frame are observed, but the

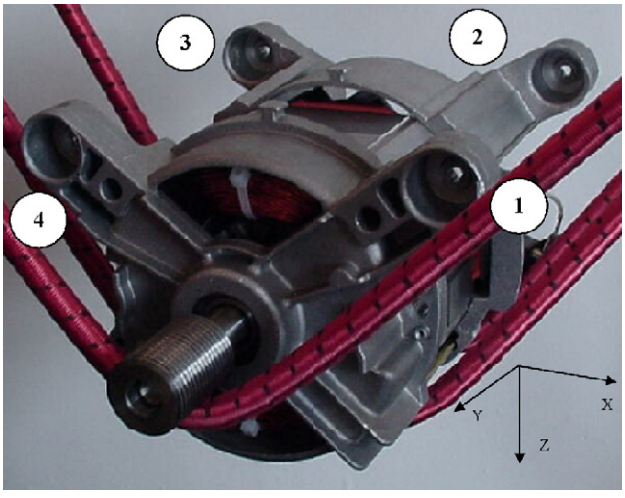

Fig. 2. The source structure, an electric motor.

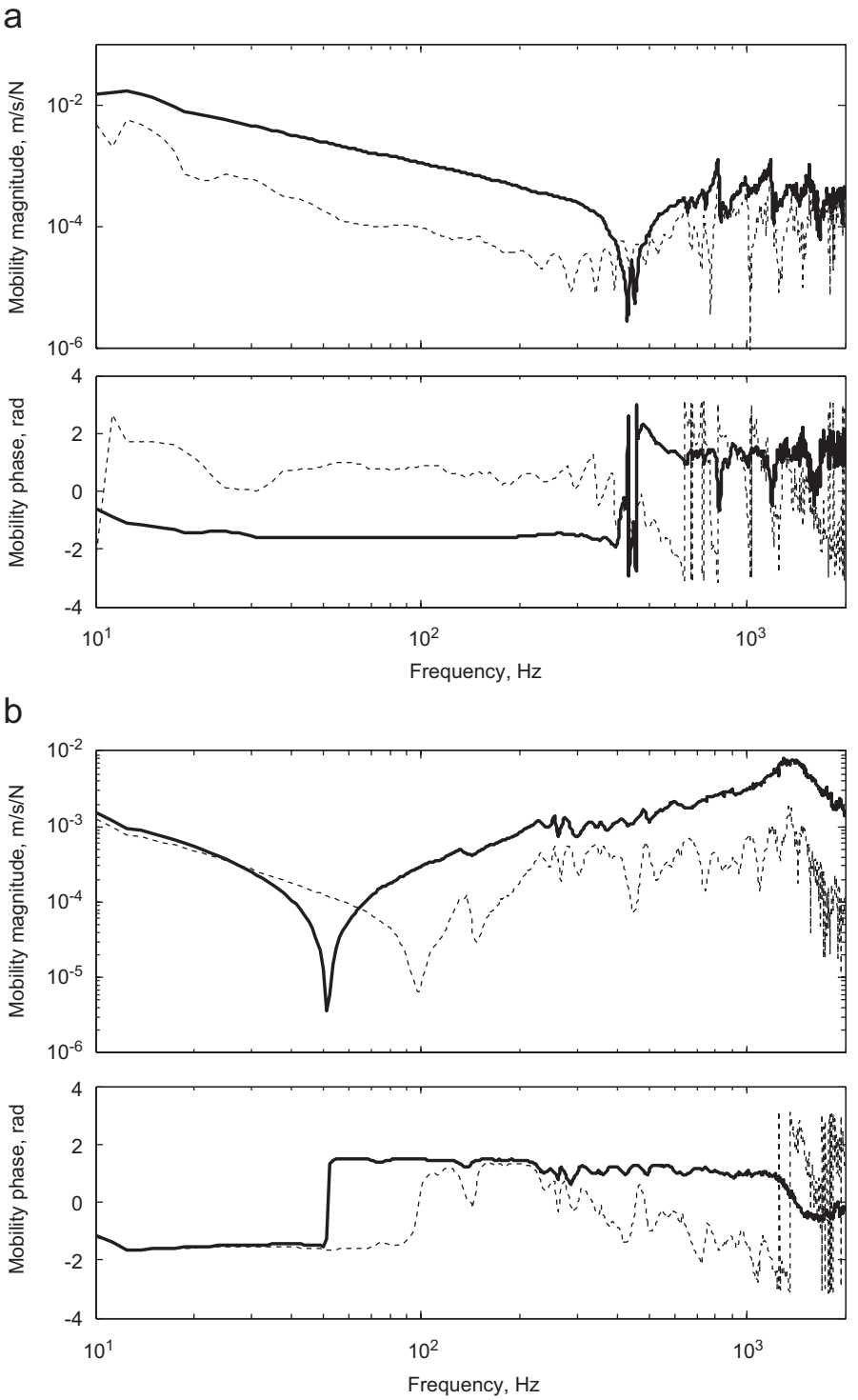

Fig. 3. Typical mobility plots for source (a) and frame (b). Bold lines are point mobility and lighter lines are typical transfer mobilities from contact point 1 in the y (axial) direction. Results for points 2, 3, 4 and x and z directions were similar and are not shown for brevity.

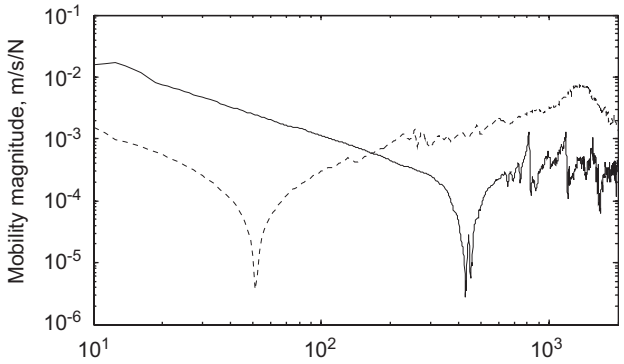

Fig. 4. Comparison of source and frame point mobility magnitude for point 1, y direction. __ source; ..... frame.

average trend is flat indicating that the behaviour can be considered to be plate-like. The corresponding plots for the source are shown in the lower plot of Fig. 3. The low-frequency behaviour is again mass-like, up to 50 Hz where an anti-resonance occurs. There follows a region of stiffness-like behaviour covering a large part of the frequency range of interest up to about 1500 Hz where there is a resonance peak. Stiffness-like behaviour is most clear between 100 and 300 Hz, and the transfer mobility in this stiffness range is comparatively low, i.e. coupling between mount points is relatively weak as has been observed for stiffness-like behaviour in other situations [24].

It has been shown in Ref. [2] that the matching between source and receiver mobility is of great importance in the power transmission. Consequently, it is instructive to compare the point mobilities of source and frame, which is done in Fig. 4 for point 1 and the y direction. It illustrates that below about 150 Hz the source mobility is higher (the source is lighter than the frame), and above this frequency the frame mobility is higher (it is more compliant than the source). This general trend was similar for other positions and directions.

3.2. Evaluation of errors using singular values

It has been observed above that the singular values of the mobility matrices are an important factor in determining the error. These are plotted in Fig. 5 for the source (upper plot) and the frame (lower plot), and reveal interesting aspects of the physical behaviour of the two structures. If the range of the singular values is narrow, then the velocity response of the structure is sensitive only to the magnitude of the exciting forces. On the other hand, a wide range in the singular values indicates that small variations in the spatial distribution of the forces could have a pronounced effect on the velocity response. These relationships were first outlined in Ref. [10]. Looking at the lower half of Fig. 5 we observe that the range is wide for the frame below 100 Hz, indicating that different distributions of the forces could produce dramatically different responses. This is because the structure is mass-like in this region, and has six degrees of freedom, so there are some combinations of 12 forces that would produce no response, while more 'efficient' distributions may produce a large effect. At higher frequencies the range of the singular values is considerably smaller, particularly between 100 and 300 Hz. It has already been observed that the transfer mobilities are low in this region, so that the points are not well coupled and act more or less independently. Furthermore, since the points are all geometrically similar, the resulting mean square velocity will be more or less the same no matter how the forces are distributed, hence the low range in the singular values.

The singular values will now be used to determine the likely error in simplifying the mobility matrices. Shown in bold in Fig. 6 are the singular values of the matrix $[\mathbf{Y}_S + \mathbf{Y}_R]$ unmodified. This matrix was then modified by removing the off-diagonal elements of $\mathbf{Y}_R$, which is equivalent to assuming that the contact points on the frame are uncoupled. The singular values were then recalculated and are shown in dotted lines. It is seen that the 'perturbed' singular values agree well with the 'true' values at low and high frequency, but that there are some differences in the range of 150–350 Hz. These results can be explained as follows. As observed in Fig. 4, at low frequencies (mass region) the source mobilities are significantly higher than those of the frame.

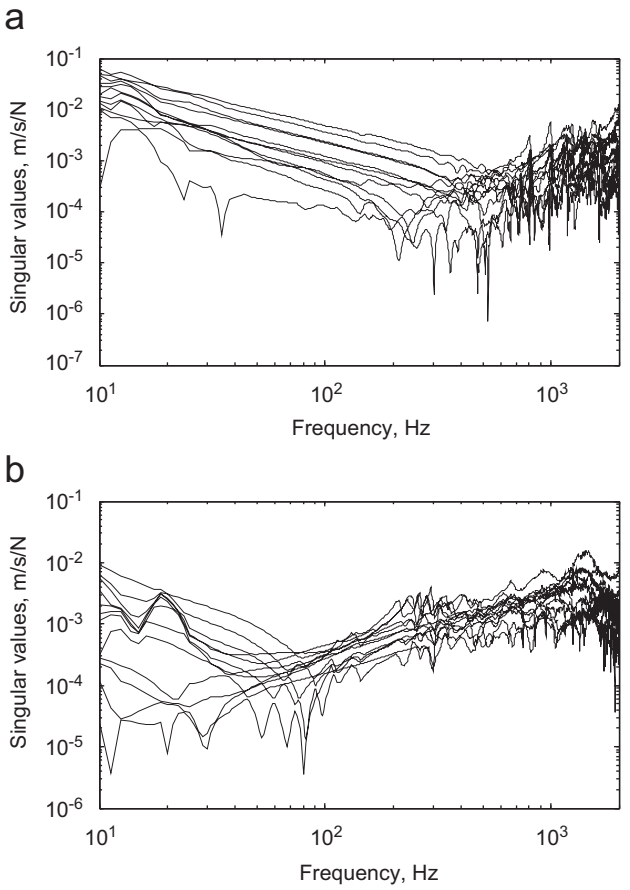

Fig. 5. Singular values of mobility matrix for source (a) and frame (b).

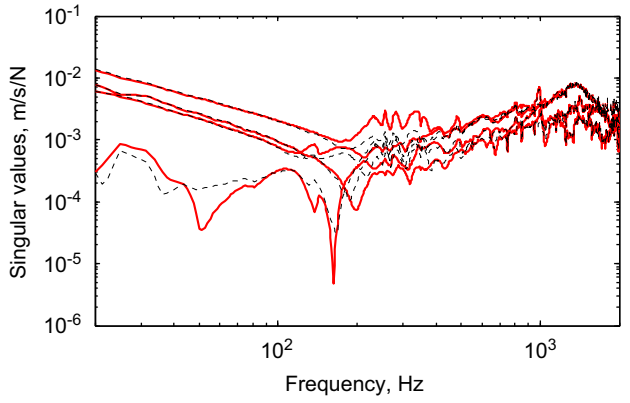

Fig. 6. Singular values of modified and unmodified mobility matrices. _____ Singular values of $[\mathbf{Y}_S + \mathbf{Y}_R]$, ... singular values of $[\mathbf{Y}_S + \text{diag}(\mathbf{Y}_R)]$, i.e. off-diagonal elements of frame mobility matrix $\mathbf{Y}_R$ removed.

Hence any of the terms in $\mathbf{Y}_R$ can be neglected without introducing significant errors. At high frequencies, the frame is less stiff than the motor, so the sum $[\mathbf{Y}_S + \mathbf{Y}_R]$ is dominated by the $\mathbf{Y}_R$ terms. However, the frame transfer mobilities (off-diagonal terms of $\mathbf{Y}_R$) are only significant compared with the diagonals in the range 150–350 Hz. Hence, this is the only frequency range where a perturbation is seen.

Fig. 6 suggests that the errors due to this simplification will be relatively small. However, it would be preferable to produce confidence limits, which demands a Monte–Carlo approach as described in the next section.

3.3. Evaluation of errors using Monte Carlo methods

Various simplifications were tested as summarised in Table 1. Neglecting off-diagonals will be valid if the transfer mobilities between points are small in comparison to the diagonals. It will also be valid if off-diagonal contributions to $|\mathbf{f}|^2$ cancel, which will tend to happen when contact points are separated by more than a wavelength due to phase differences. Neglecting $\mathbf{Y}_S$ assumes that the source is not dynamically 'loaded' by the frame, and is equivalent to the velocity source assumption.

Eq. (9a) was evaluated using 100 random vectors for each case. This was shown to be a sufficient sample size by carrying out a preliminary check with an increasing number of vectors until convergence was obtained. The predicted normalised forces squared at each frequency were arranged in ascending order and the 5th and 95th estimates were plotted as a function of frequency, as shown in Fig. 7 for Mod 1. These values correspond to the 90% confidence limits on the normalised force squared, i.e. there is a 90% probability that the ratio of the simplified and exact prediction of $|\mathbf{f}|^2$ will occur between the two lines. Similar results for Mods 2–5 are shown in Fig. 8.

The results of stripping the off-diagonals from the frame mobility matrix are shown in Fig. 7. The singular values for this case have already been discussed in Fig. 6, from which it was expected that this simplification would produce a relatively small error except in the range 150–350 Hz and below about 80 Hz. The confidence limits in Fig. 7 are consistent with this expectation. This result was also anticipated from consideration of the transfer mobilities (Fig. 3) which were relatively small, indicating generally weak coupling between points on the frame. The implications of these results are that off-diagonal terms of the frame matrix can be fairly safely neglected, which would substantially reduce the measurement, data handling and processing effort required to calculated forces. It should be appreciated that the confidence limits are if anything conservative since it is assumed that any excitation vector $\mathbf{q}$ is equally likely; in practise there will always be some restriction on $\mathbf{q}$ (such as in rigid mass behaviour as discussed earlier) which will reduce the range of errors. Furthermore, as argued in relation to Eq. (3b), if the excitation forces are incoherent the contribution of cross terms, and hence errors, will diminish.

Fig. 8(a) shows the corresponding results when assuming the source mobility matrix to be diagonal. Significant errors occur in the range $200\,\text{Hz} < f < 600\,\text{Hz}$. Not only is there a large spread but there is a bias error, so, for example we can be 90% confident that there will be an underestimate of at least 8 dB at 400 Hz. It is interesting that above 600 Hz the errors are relatively small. This would not necessarily be predicted from consideration of the transfer mobilities which are of similar magnitude to the point mobilities. A possible explanation is that although there is significant interaction between contact points, the contributions to the response from other points tends to cancel because of differing phases (see discussion following Eq. (3b)).

Fig. 8(b) shows the corresponding results for the velocity source assumption. This simplification introduces a bias error over most of the frequency range. The large overestimate at low frequencies can be explained by

Table 1
Summary of simplifications tested

Number	Simplification	Interpretation
Mod 1	$\mathbf{Y}_R \rightarrow \text{diag}(\mathbf{Y}_R)$	Valid either if the coupling between frame contact points is small, or if the phase of the coupling terms is random
Mod 2	$\mathbf{Y}_S \rightarrow \text{diag}(\mathbf{Y}_S)$	Valid either if the coupling between motor feet is small, or if the phase of the coupling terms is random
Mod 3	$\mathbf{Y}_S \rightarrow 0$	Equivalent to velocity source assumption
Mod 4	Use y direction data for $\mathbf{Y}_R$	x and z mobilities replaced by y data. Assumes mobility similar in each direction
Mod 5	Use y direction data for $\mathbf{Y}_S$	As above for source

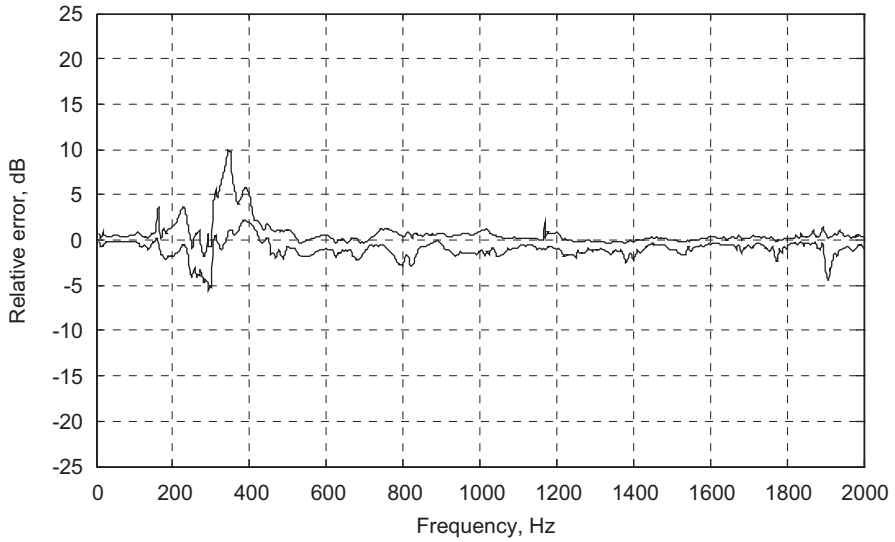

Fig. 7. 90% confidence limits for prediction of $|\mathbf{f}|^2$ for Mod 1, $\mathbf{Y}_R \rightarrow \text{diag}(\mathbf{Y}_R)$.

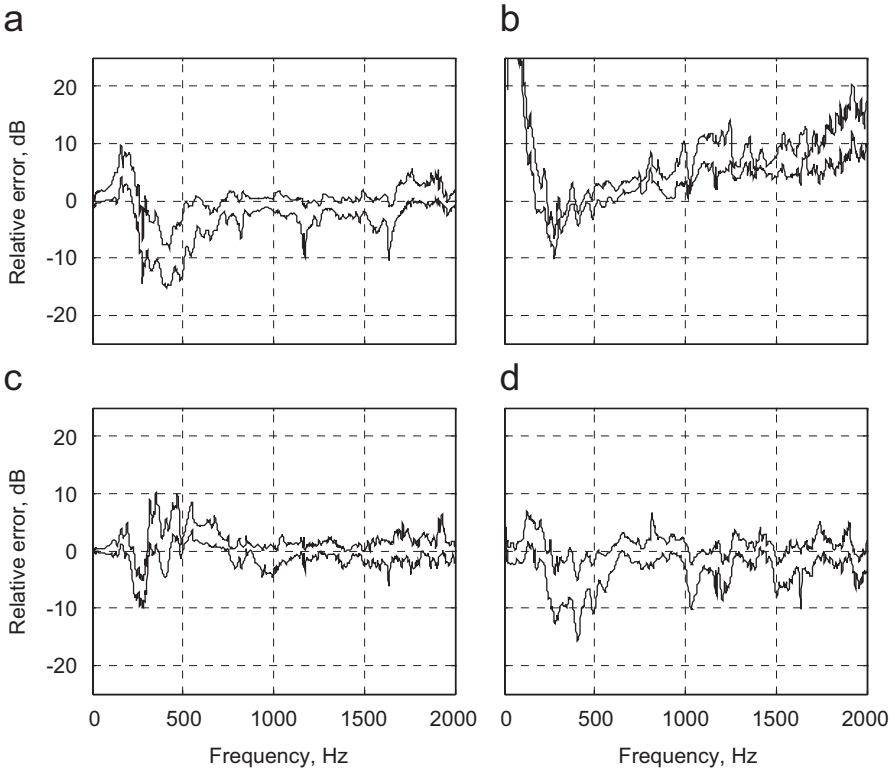

Fig. 8. 90% confidence limits for prediction of $|\mathbf{f}|^2$ for (a) Mod 2, $\mathbf{Y}_S \rightarrow \text{diag}(\mathbf{Y}_S)$, (b) Mod 3, $\mathbf{Y}_S \rightarrow 0$, (c) Mod 4 ($y$ direction data for $\mathbf{Y}_R$), (d) Mod 5 (y direction data for $\mathbf{Y}_S$).

consideration of Fig. 4: the mass of the frame is significantly higher than that of the source, so there is a large reduction in velocity when the source is connected to the frame. Above about 350 Hz, Fig. 4 suggests that the loading of the source by the frame might be minimal because there is a 10 dB offset in the magnitudes of their

point mobilities. However, Fig. 8(b) shows that there is in fact significant loading when all points and directions are taken into account, and the free velocity is an overestimate of the coupled velocity.

Shown in Figs. 8(c) and (d) are the results of assuming the x and z mobilities to be equal to the y mobilities for the frame and source, respectively. The logic of this simplification is that it had previously been noted that there were no large differences in the mobilities in each direction, so to measure only one direction might be sufficient and would give a reduction in the measurement and data handling. The errors are relatively small, except below 200 Hz in Fig. 8(d), i.e. when the source mobilities are approximated. The higher errors in this region are understandable since this is the region of rigid mass behaviour and the mobility would be expected to vary with direction.

3.4. Interpretation of results

From Fig. 8(b), both source and frame mobility must be taken into account. Fig. 7 shows that only the diagonal elements of the frame mobility need to be included. For the source, the off-diagonals can be neglected above 600 Hz. However, below 600 Hz they must be included, and the points on the motor should be considered as coupled. This 600 Hz limit is specific to the particular motor. However, a more general conclusion can be drawn by noting from the point mobility curves of the motor (Figs. 3 and 4) that it behaves as a rigid mass up to about 200 Hz, and that there is an anti-resonance between 200 and 600 Hz. Therefore, the frequency region over which coupling must be considered includes mass-like and anti-resonant behaviour. This type of behaviour is often, almost invariably, displayed for sources, so we can argue that the conclusions will probably also be true for other types of sources irrespective of the absolute frequency over which this behaviour occurs. Therefore, the conclusion is that coupling must be included at low frequencies where the structure behaves as a rigid body up to at least the 'end' of the first anti-resonance.

Fortunately, the overall behaviour in this frequency region is relatively simple and the matrix should be readily calculable. Therefore, it is proposed to use a hybrid matrix for the motor wherein, at low frequency the entire matrix is populated by calculated values, and, at high frequencies only diagonal values are used, i.e. measured point mobilities.

3.5. Evaluation of errors in radiated sound pressure

Before testing the proposed hybrid mobility matrix, it is worthwhile to consider the errors in radiated sound pressure. These can be evaluated in a similar manner as was done for the forces above, using Eq. (3) as a starting point. The normalised sound pressure squared then becomes:

$$E_p = \frac{\mathbf{f}'^H \mathbf{T}^H \mathbf{T} \mathbf{f}'}{\mathbf{f}^H \mathbf{T}^H \mathbf{T} \mathbf{f}}, \tag{10}$$

where the numerator represents the modified case and the denominator the reference, unmodified case. The unmodified force vectors $\mathbf{f}$ are calculated from Eq. (2a), and similarly for the modified vector $\mathbf{f}'$. The 6×12 matrix of transfer functions $\mathbf{T}$, which is not modified, was obtained by a reciprocal measurement technique. Here, a volume velocity source is placed at the external positions and the velocity level on the frame at the contact points in x, y and z directions is measured (see Ref. [24] for a brief description of the measurements).

Fig. 9 shows the calculated bounds on the normalised sound pressure squared for Mod 2, i.e. off-diagonals of the source mobility matrix neglected. The grey-scale shaded area gives the 90% confidence limits for the normalised sound pressure squared, and the solid lines give the corresponding results in the force, which are the same results as given in Fig. 8(a). It is seen that the errors in pressure follow the same trends as for the force, but with slightly broader bands. Results for other modifications were similar and are not shown. These results justify the approach of focusing on the effect of simplifications on the calculated forces.

4. Use of a hybrid measured and calculated mobility matrix

The mobility matrix in the rigid body region can be calculated based on simple geometric parameters, namely, the offset of the contact points from the centre of gravity, the mass and the radius of gyration in the x,

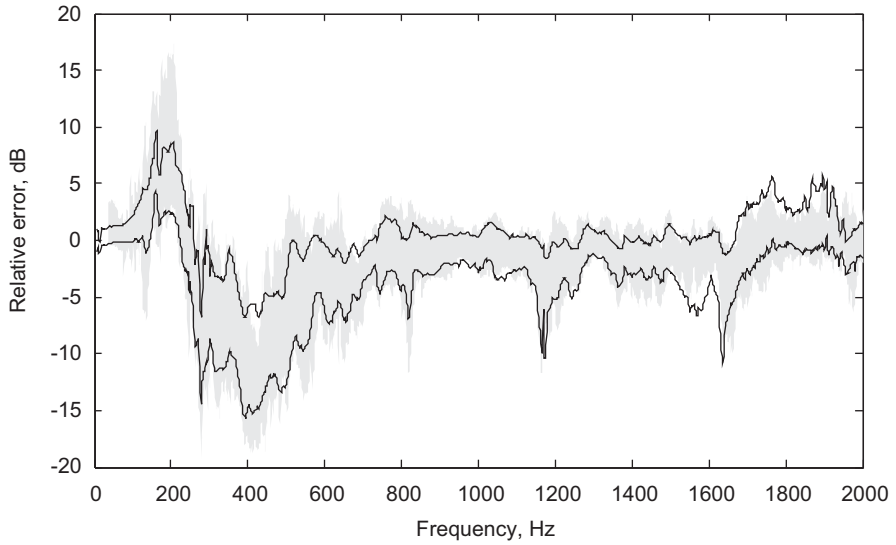

Fig. 9. 90% confidence limits for prediction of $|\mathbf{f}|^2$ (lines); for $|\mathbf{p}|^2$ (greyscale shaded area), for Mod 2, $\mathbf{Y}_S \rightarrow \mathrm{diag}(\mathbf{Y}_S)$.

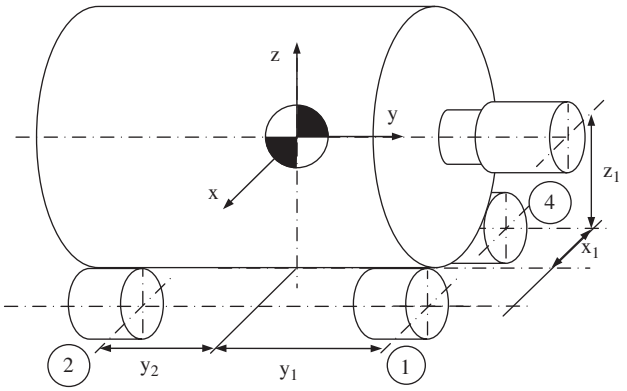

Fig. 10. Geometry of the motor.

y and z directions as illustrated in Fig. 10. A general term in the accelerance matrix for a rigid mass excited in the y direction is given by [19,24]

$$\frac{a_{y,i}}{f_{y,j}} = \frac{1}{m}\left[1 + \frac{x_i x_j}{p_z^2} + \frac{z_i z_j}{p_x^2}\right], \tag{11}$$

where $a_{y,i}$ is the acceleration at point i due to a force $f_{y,j}$ at point j with all other forces zero; m is the mass of the motor, p_x and p_z are the radii of gyration for rotation about the x and z axes, respectively, and x_i, z_i and x_j, z_j are the offsets of the response and excitation points respectively from the centre of gravity as shown in Fig. 10. Eq. (11) can conveniently by extended to matrix–vector form to give the mass mobility matrix for excitation and response in the y direction:

$$\mathbf{A}_{yy} = \frac{1}{m}\left[\mathbf{U} + \frac{1}{p_z^2}\mathbf{x}\mathbf{x}^{\mathrm{T}} + \frac{1}{p_x^2}\mathbf{z}\mathbf{z}^{\mathrm{T}}\right], \tag{12}$$

where $\mathbf{U}$ is an $n \times n$ square matrix of ones, and $\mathbf{x}$, $\mathbf{z}$ are column vectors of the offsets of the contact points from the centre of mass. Similar matrices apply for motion in the x and z directions.

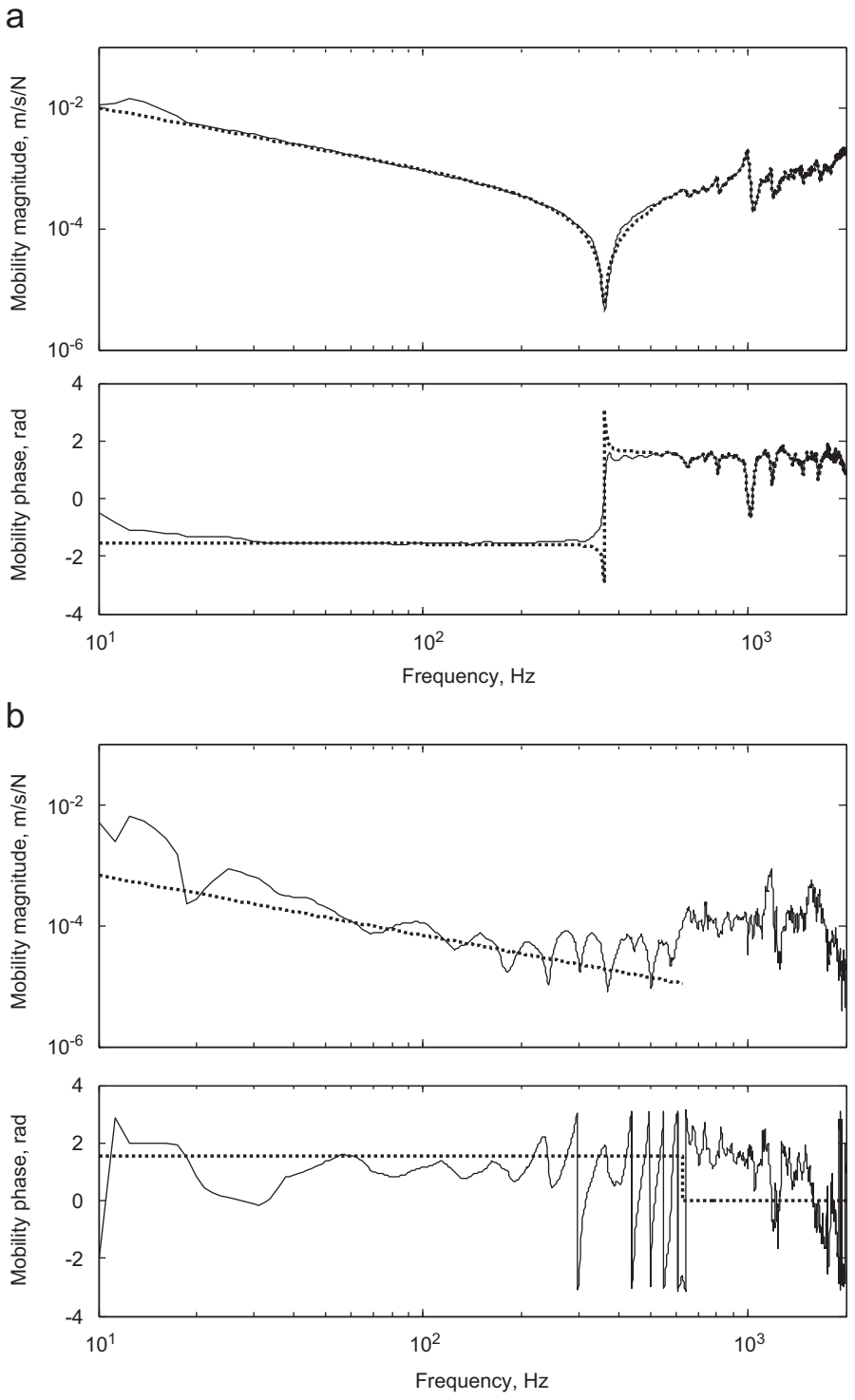

Fig. 11. ___measured and ..... hybrid mobility curves. (a) point mobility; (b) transfer mobility.

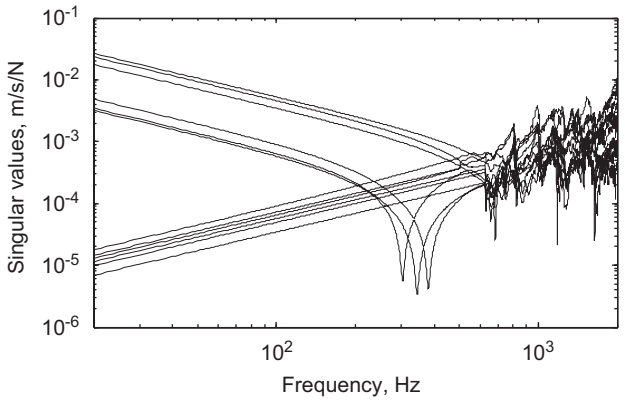

Fig. 12. Singular values of the hybrid mobility matrix.

For excitation in the y direction there is also a response in the x and z directions in general. These cross terms are given by

$$\frac{a_{z,i}}{f_{y,j}} = \frac{1}{m}\left[\frac{-y_i z_j}{p_x^2}\right], \quad \frac{a_{x,i}}{f_{y,j}} = \frac{1}{m}\left[\frac{-y_i x_j}{p_z^2}\right], \tag{13}$$

where symbols are as above, but with the addition of y_i, which is the y direction offset of the response point from the centre of gravity.

Again, this can be extended to an arbitrary number of points by writing in matrix form:

$$\mathbf{A}_{zy} = \frac{-1}{mp_x^2}\mathbf{y}\mathbf{z}^{\mathrm{T}}, \quad \mathbf{A}_{xy} = \frac{-1}{mp_z^2}\mathbf{y}\mathbf{x}^{\mathrm{T}}, \tag{14}$$

where $\mathbf{y}$ is the column vector of the y direction offsets of the excitation points from the centre of mass. Similar expressions apply for the other directions. The whole accelerance matrix for the mass-like region of behaviour can then be assembled:

$$\mathbf{A} = \begin{bmatrix} \mathbf{A}_{xx} & \mathbf{A}_{xy} & \mathbf{A}_{xz} \\ \mathbf{A}_{yx} & \mathbf{A}_{yy} & \mathbf{A}_{yz} \\ \mathbf{A}_{zx} & \mathbf{A}_{zy} & \mathbf{A}_{zz} \end{bmatrix}. \tag{15}$$

Values for the $\mathbf{x}$, $\mathbf{y}$ and $\mathbf{z}$ can be obtained by geometry as shown in Fig. 10, provided the position of the centre of mass is known with reasonable accuracy. The radii of gyration will not generally be known, but can be estimated based on a few measured transfer mobilities by using Eq. (11). Thus, the accelerance matrix for rigid body behaviour can be calculated.

In order to calculate the mobility matrix in the anti-resonant region, it is necessary to combine the calculated mass-mobility matrix with a compliance-mobility matrix. The total mobility matrix is then formed by the complex addition of the two, i.e.:

$$\mathbf{Y}_S = \frac{1}{j\omega}\mathbf{A} + j\omega\mathbf{C}, \tag{16}$$

where $\mathbf{A}$ is the accelerance matrix calculated from Eqs. (12), (14) and (15), and $\mathbf{C}$ is a compliance matrix:

$$\mathbf{C} = (1 - \mathrm{j}\eta)\mathrm{diag}\left[1/k_i\right] \tag{17}$$

in which the k_i are the stiffnesses of points 1–4 on the motor, and η is the loss factor. This matrix is assumed diagonal, since, as remarked previously, it is known that off-diagonal elements are usually small in regions of stiffness-like behaviour [25]. (One possible exception is shell structures with points closely spaced compared with a free wavelength.)

Anti-resonances occur when the diagonals of **A** and **C** are of equal magnitude. Values for the stiffnesses k_i were found from measured point mobilities by fitting the anti-resonance frequency calculated from Eq. (5a), to the measured point mobility. To obtain the loss factor, a trial value was employed and adjusted until the sharpness of the anti-resonance dip agreed with the measured curve. The complete data set for calculating the low-frequency part of the mobility matrix (y direction) consists of a small number of parameters: the mass, loss factor, x, y and z offset of feet from the centre of mass, radii of gyration about x, y and z axes, stiffnesses in three directions for front and back feet.

Fig. 11 shows the measured mobility magnitude curve, together with a hybrid curve consisting of the curve-fitted values below anti-resonance and measured values above. The frequency for changeover from calculated to measured mobilities was set where the anti-resonant behaviour was judged by eye to be 'completed', and was 630 Hz for points 1 and 4, and 505 Hz for points 2 and 3. The calculated curve is seen to capture the

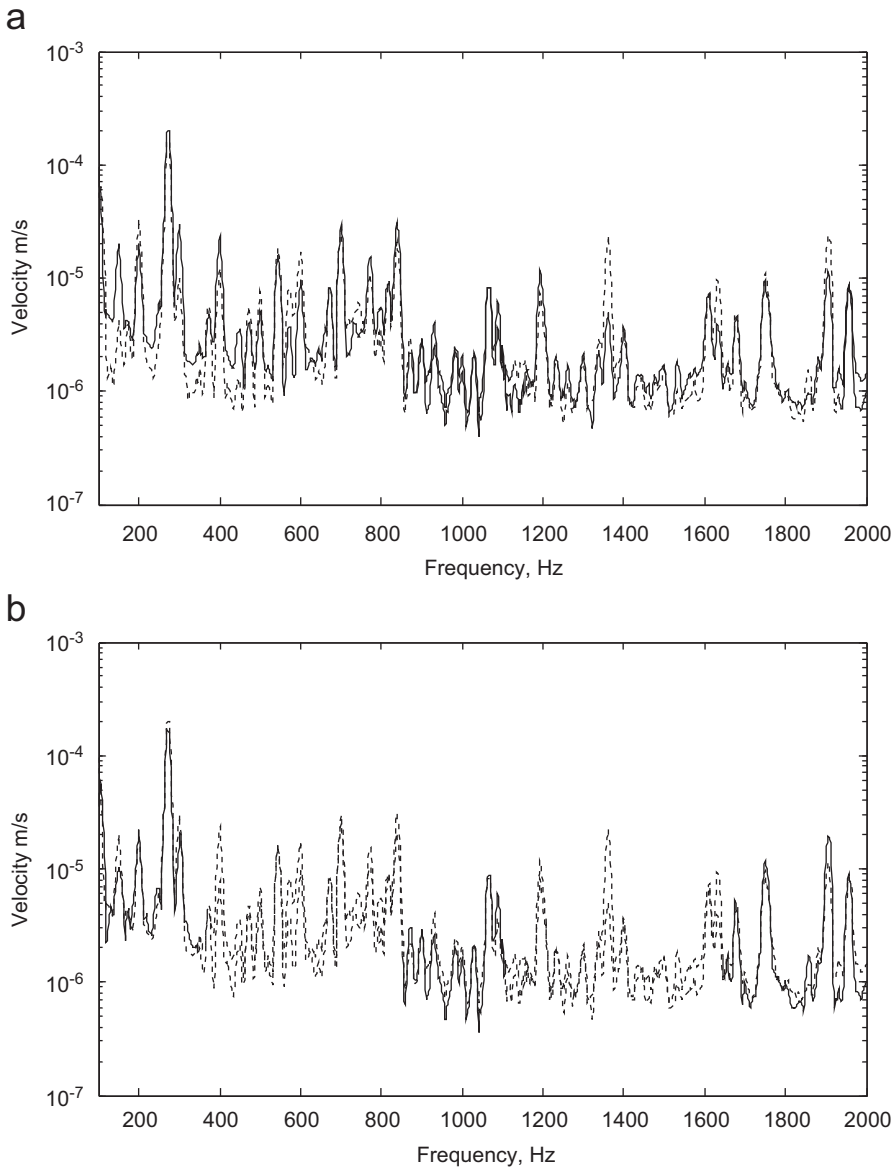

Fig. 13. Comparison of ____ measured and ..... predicted coupled velocity for 16500 rev/min. (a) Prediction using full measured mobilities; (b) prediction using hybrid mobility matrix for source.

essential behaviour but is 'cleaner' than the measured one. Indeed, it can be argued that the calculated curve is a more faithful representation of the true behaviour being based on more robust physical characteristics, particularly in the anti-resonant region and at low frequencies where measurement errors can be significant.

Shown in Fig. 12 are the singular values for the hybrid matrix. The low-frequency asymptotes give six non-zero singular values: the largest three of these correspond to rotations of the mass about three perpendicular axes (not as it happens coinciding with x, y and z), and the lower non-zero set of three correspond to rigid body translation in the x, y and z directions. These can be compared with those from the measured matrix given in the upper plot of Fig. 5. Here the low-frequency asymptotes suggest there are 12 independent degrees of freedom which is physically wrong. This strengthens the argument that the calculated matrix is more accurate than the measured one.

To summarise, the hybrid mobility matrix for the source is fully populated by calculated values below 600 Hz. Above this frequency, the matrix is diagonal consisting of only the measured point mobilities. Thus, the entire matrix is constructed from only measured point mobilities. This is significantly simpler than using the full matrix in terms of measurement, and more importantly, data handling. It remains to be seen whether the simple matrix gives sufficiently accurate predictions.

5. Validation of the hybrid matrix

In order to validate the hybrid matrix, the motor was mounted in the machine frame and the velocity at the contact points measured. This 'coupled velocity' was also predicted:

(a) using the 12×12 measured mobility matrix for source and receiver,
(b) using simplified matrices, i.e. the 12×12 hybrid matrix for the source and frame.

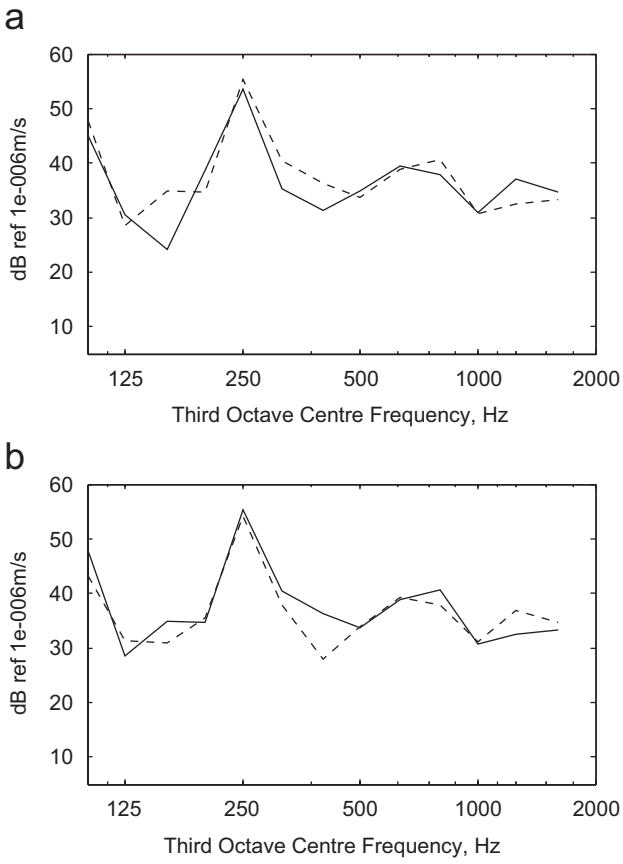

Fig. 14. As Fig. 13, but third octave values.

The coupled velocity was calculated from:

$$\mathbf{v}_c = \mathbf{Y}_R\mathbf{f} = \mathbf{Y}_R[\mathbf{Y}_S + \mathbf{Y}_R]^{-1}\mathbf{v}_{sf}, \tag{18}$$

where $\mathbf{v}_c$ is the coupled velocity vector and other terms have been defined previously. Tikhonov regularisation was used for the matrix inversion with the regularisation parameter β set to 0.05 times the mean of the singular values squared. Although the calculations were carried out using 12×12 matrices, only the y direction coupled velocity was measured and included in the comparison, i.e. the comparison was made on the basis of a subset of results, which is valid.

A sample of the results is shown in Fig. 13 for a running speed of 16,500 rev/min. The spectra are seen to consist of a harmonic series and are typical for an electric motor. Fig. 14 shows the same results but in third octave bands (which are shown to aid comparison). The upper plots of Figs. 13 and 14 show the calculation

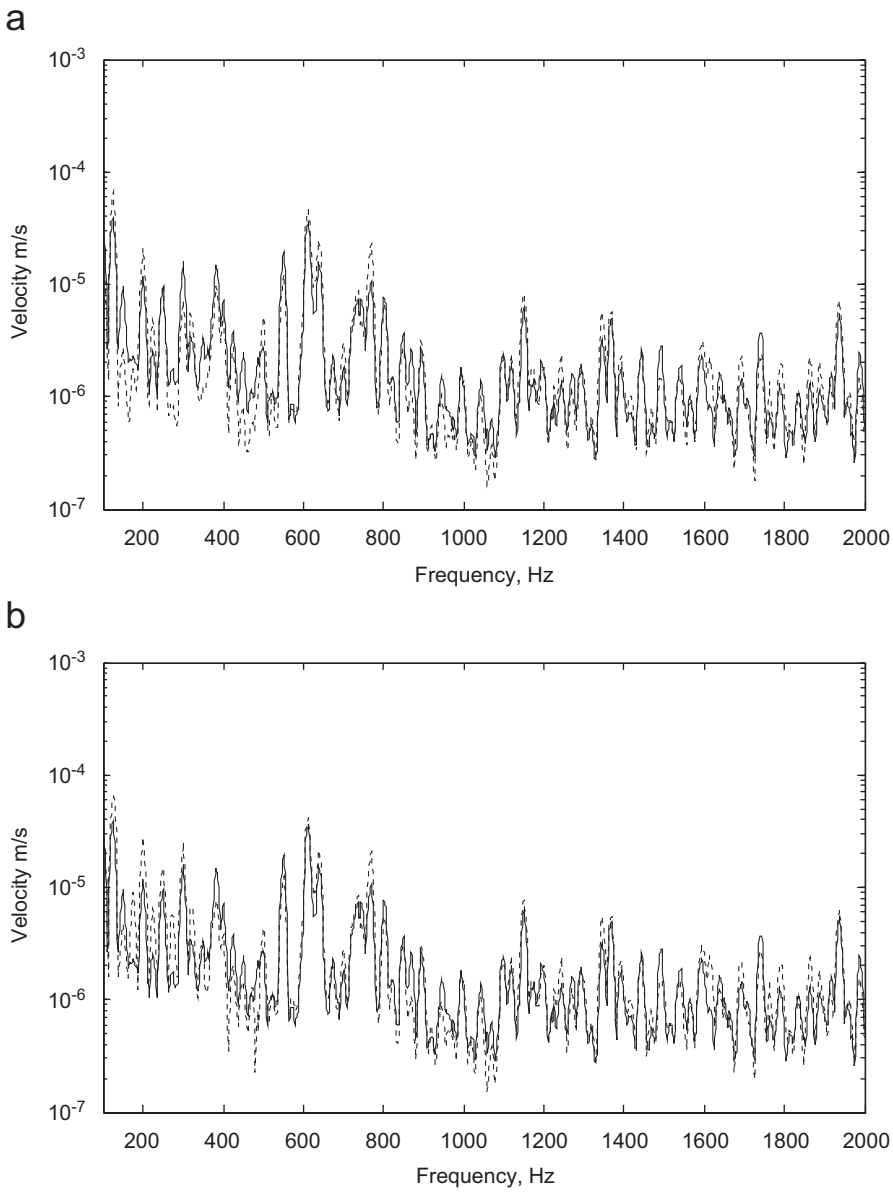

Fig. 15. Comparison of ____ measured and ..... predicted coupled velocity for 7600 rev/min. (a) Prediction using full measured mobilities; (b) prediction using hybrid mobility matrix for source.

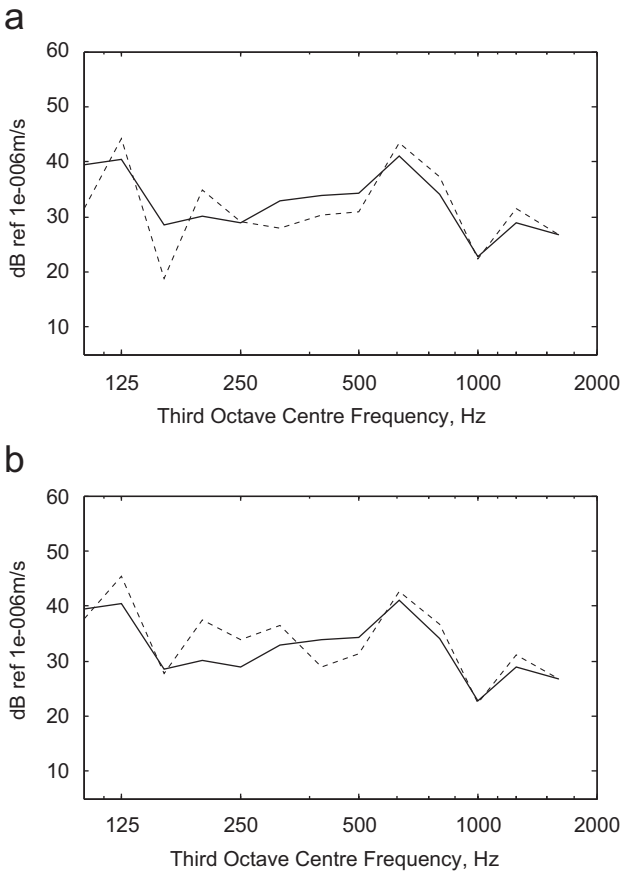

Fig. 16. As Fig. 15, but third octave values.

from the full mobility matrix compared with direct measurement and the lower plots those from the hybrid matrix. Firstly, it is noted that both full and simplified predictions give good agreement with direct measurement. Secondly, as predicted in the sensitivity analysis above there are no major discrepancies introduced by the simplification. Thus, although the simplified matrices use far less measured data they do not generally provide less accurate predictions. Indeed, in the lowest frequency bands the predictions are more accurate, for example, the lowest frequencies of Figs. 13 and 14. This was already anticipated from above where physical behaviour dictates there should be only 6 non-zero singular values, whereas the measured results showed there to be 12.

Above 500 Hz the simplification consisted of removing all but the diagonal elements. Here the accuracy is good, which was anticipated from the confidence limits in Fig. 8, despite the fact that a conventional examination of the transfer mobilities from Fig. 4 suggests strong coupling between contact points in the source. This is taken to indicate that the cross terms tend to cancel due to random phase.

Figs. 15 and 16 show similar results for a lower running speed of 7600 rev/min. The results and conclusions are essentially the same as above. Other running speeds were also examined and yielded generally similar results which are not shown.

6. Concluding remarks

The background to this work is increased interest in virtual acoustic prototypes. Here, the sound pressure from an assembled machine is calculated from two independent data sets, one characterising the properties of the vibro-acoustically active components, and another representing the properties of the remaining passive parts of the machine. The focus of the paper is on structure-borne sound transmission, and particularly on the

calculation of contact forces between the active component and its supporting structure. Various ways have been investigated of reducing the large quantity of data needed to calculate the contact forces, and the errors caused by the simplifications have been tested using both singular value expansions and Monte Carlo simulations. It has been argued that the errors in the contact forces due to simplification are to a large extent representative of the errors in the subsequently radiated sound pressure.

The confidence limits produced showed that it is possible to neglect off-diagonal elements of the source mobility matrix above the first anti-resonance frequency. However, at low frequencies, no elements of the matrices could be neglected without introducing significant errors. It was observed that the region of large errors corresponded with the frequency range in which the source behaves as a rigid mass. It was therefore proposed that the low-frequency behaviour be calculated from a rigid mass model, combined with local stiffness of the feet. Measured point mobilities were used to obtain the radii of inertia and the local stiffness required for the model. At frequencies above the first anti-resonance the simple model is not valid, and measured point mobilities were used.

The hybrid mobility matrix was validated by calculating the coupled velocity of the motor when rigidly attached to its frame, and comparing with the measured velocity. No loss of accuracy was caused by the simplification; indeed, in some cases the simplified predictions were more accurate. It is argued that this is because the predicted mobilities in the mass region are more robust than measured values, being based on more simple characteristics like mass and geometry.

The proposed hybrid approach allows all the necessary mobility data to be obtained purely from measured point mobilities, with no need to measure transfer mobilities. This represents a significant reduction in the measured, and more importantly data handling effort required.

Although in this paper only a single structure-borne source has been considered, it has been argued that the same approach is likely to be applicable to other cases of practical importance.

Acknowledgements

This work was partly carried out within EC-funded project NABUCCO (GRD–1999-10785). Funding by the European Commission is gratefully acknowledged.

References

[1] L. Cremer, M. Heckl, E.E. Ungar, *Structureborne Sound*, Springer, Berlin, 1973.
[2] J.M. Mondot, B.T. Petersson, Characterization of structure-borne sound sources: the source descriptor and the coupling function, *Journal of Sound and Vibration* 114 (3) (1987) 507–518.
[3] R.A. Fulford, B.A.T. Petersson, 1997 Estimation of vibrational power in built-up systems involving box-like structures, part 1: uniform force distribution, *Journal of Sound and Vibration* 232 (5) (2000) 877–895.
[4] B.A.T. Petersson, A.T. Moorhouse, Interface mobilities for source characterisation; matched conditions, *Proceedings of the Seventh ICA*, Rome, 2001.
[5] J.M. Mondot, A.T. Moorhouse, The characterisation of structure-borne sound sources, *Proceedings of Inter-noise 96*, Book 3, Liverpool, 1996, pp. 1439–1446.
[6] L. Ji, B.R. Mace, R.J. Pinnington, Estimation of power transmission to a flexible receiver from a stiff source using a power mode approach, *Journal of Sound and Vibration* 268 (3) (2003) 525–542.
[7] B.M. Gibbs, A.T. Moorhouse, Case studies of machine bases as structure-borne sound sources in buildings, *International Journal of Acoustics and Vibration* 4 (3) (1999).
[8] B.A.T. Petersson, B.M. Gibbs, Towards a structure-borne sound source characterization, *Applied Acoustics* 61 (3) (2000) 325–343.
[9] S. Jianxin, A.T. Moorhouse, B.M. Gibbs, Towards a practical characterisation for structure-borne sound sources based on mobility techniques, *Journal of Sound and Vibration* 185 (4) (1995) 737–741.
[10] A.T. Moorhouse, B.M. Gibbs, Simplified characterisation of multiple point excited structures using mobility matrix eigenvalues and eigenvectors, *Acustica united with Acta Acustica* 84 (5) (1998) 843–853.
[11] L. Ji, B.R. Mace, R.J. Pinnington, A power mode approach to estimating vibrational power transmitted by multiple sources, *Journal of Sound and Vibration* 265 (2) (2003) 387–399.
[12] R.J. Pinnington, D.C.R. Pearce, Multipole expansion of the vibration transmission between a source and a receiver, *Journal of Sound and Vibration* 142 (3) (1990) 461–479.
[13] B.A.T. Petersson, Geometrical and spatial effects on effective mobilities of annular interfaces, *Journal of Sound and Vibration* 202 (4) (1997) 511–537.

[14] G. Pavic, A.T. Moorhouse, Is virtual acoustic prototyping simply a noise prediction tool? *Proceedings of Inter-noise 2004*, Prague, Czech Republic, 2004.
[15] G. Pavic, L. Gavric, J. Tourret, R. Sottek, Noise synthesis from a fan-type source placed in complex installation, *Proceedings of Fan Noise 2003*, Senlis France, 2003.
[16] J.H. Wilkinson, *The Algebraic Eigenvalue Problem*, Oxford University Press, London, 1965.
[17] A.T. Moorhouse, A dimensionless mobility formulation for evaluation of force and moment excitation of structures, *Journal of Acoustics Society of America* 112 (2002) 972.
[18] L. Ji, B.R. Mace, R.J. Pinnington, A power mode approach to estimating vibrational power transmitted by multiple sources, *Journal of Sound and Vibration* 265 (2) (2003) 387–399.
[19] A.T. Moorhouse, R.D. Cookson, G. Seiffert, Measurement of operating forces of an electric motor, *Proceedings of NOISE-CON 2004*, Baltimore, USA, 2004.
[20] S. Jianxin, Simplified characterisation of structure-borne sound sources with multi-point connections, PhD Thesis, University of Liverpool, 2003.
[21] A.T. Moorhouse, Use of a hybrid measured-calculated mobility matrix for simplified calculation of structure-borne sound from an electric motor, *Proceedings of the 10th ICSV*, Stockholm, 2003.
[22] G.H. Golub, C.F. Van Load, *Matrix Computations*, Johns Hopkins University Press, Baltimore, 1983.
[23] R.A. Fulford, B.M. Gibbs, Structure-borne sound power and source characterization in multi-point-connected systems. part 3: force ratio estimates, *Journal of Sound and Vibration* 225 (2) (1999) 239–282.
[24] R.A. Fulford, B.M. Gibbs, Structure-borne sound power and source characterization in multi-point-connected systems, part 2: about mobility functions and free velocities, *Journal of Sound and Vibration* 220 (2) (1999) 203–224.
[25] A.T. Moorhouse, G. Seiffert, Characterisation of an airborne sound source for use in a virtual acoustic prototype, *Journal of Sound and Vibration* 296 (2006) 334–352.